Simulations of elementary processes in entangled wormlike micelles under tension: a kinetic pathway to Y-junctions and shear induced structures

2004 J. Phys.: Condens. Matter 16 S3965

(http://iopscience.iop.org/0953-8984/16/38/014)

INSTITUTE OF PHYSICS PUBLISHING JOURNAL OF PHYSICS: CONDENSED MATTER

J. Phys.: Condens. Matter **16** (2004) S3965–S3974 PII: S0953-8984(04)80648-9

Simulations of elementary processes in entangled wormlike micelles under tension: a kinetic pathway to Y-junctions and shear induced structures

W J Briels, P Mulder and W K den Otter

Computational Dispersion Rheology, Faculty of Science and Technology, University of Twente, PO Box 217, 7500 AE Enschede, The Netherlands

Received 6 May 2004
Published 10 September 2004
Online at stacks.iop.org/JPhysCM/16/S3965
doi:10.1088/0953-8984/16/38/014

Abstract

The merging process of two amphiphilic cylindrical micelles has been simulated using a coarse grained model in which amphiphiles are represented as chains of one head particle and four tail particles. In our set-up with twisted boundary conditions, a ring-shaped worm is effectively entangled with itself. Upon stretching the box, putting the worms under tension, a fusion into an H-like structure is observed, which eventually transforms into an almost tensionless structure with two freely gliding Y-junctions. The tensions on the worms never reach the point where scission becomes an alternative to fusion. We end with a short discussion of the possible implications of these observations.

1. Introduction

Depending on molecular structure and prevailing thermodynamic conditions, amphiphilic molecules self-assemble in a great variety of morphological structures. A convenient parameter to quantify the importance of the molecular structure is the packing parameter $p = v/(al)$, where v is the volume of the hydrophobic tail of the amphiphile, a is the area occupied by its hydrophilic head group and l the length of its tail. Often a crude understanding of the influence of thermodynamic parameters, such as salt concentration and temperature, on the morphology can be obtained by considering their influence on the packing parameter. In dilute solutions micellar structures tend to be spherical for values of the packing parameter around $1/3$ and rodlike when p is close to $1/2$ [1]. With increasing surfactant concentration, c_D, rodlike amphiphiles grow into long cylindrical structures or worms, whose lengths finally by far exceed their persistence lengths. The persistence length l_p is the length over which the worm may be considered to be a stiff rod. It is related to the bending rigidity coefficient κ by $l_p = \kappa/(k_B T)$, with k_B Boltzmann's constant and T the temperature. Above some overlap concentration c_D^* wormlike micellar solutions enter the semi-dilute regime, where the worms get entangled and consequently their viscosities increase dramatically. In many respects wormlike micelles may

be thought of as giant polymers or polyelectrolytes. An important difference, however, is their ability to reversibly break and recombine on experimental timescales. As a result, wormlike micelles have a rich rheology, rendering them perfect functional fluids in many industrial applications [2]. Several review papers have been published describing their rheological and structural properties [3–5], and a theoretical explanation thereof [6] which is believed to be applicable at least in the case of specific model systems. In this introduction we will restrict ourselves to mentioning a few of the basic assumptions and results relating to the possible occurrence of entanglements and Y-junctions.

Since scission energies E_{sc}, i.e. the energies to create two new end points, are typically in the order of $25k_BT$ and the corresponding activation barriers are not insurmountably large, wormlike micelles are subject to many scissions and re-combinations on the characteristic timescales of most rheological experiments. As a consequence, their length distribution may be assumed to be the thermodynamic equilibrium distribution [1, 3, 6]:

$$c(L) \sim \exp(L/\langle L\rangle)$$
$$\langle L\rangle = 2l_p\varphi^{\alpha}\exp(E_{sc}/2k_BT).$$

Here $c(L)$ is the number concentration of chains of length L, $\langle L\rangle$ is the average length, φ is the surfactant volume fraction, and α is an exponent which in the mean field approximation is equal to 0.5. Average lengths typically range from hundreds of nanometres to several micrometres; for comparison, diameters are typically a few nanometres and persistence lengths are in the order of 10–30 nm [4]. The above length distribution assumes that only linear worms occur, which can break and can recombine when two endpoints meet. On the basis of a variety of rheological experiments, several authors [7–9] have suggested that branching of worms and the formation of saturated networks may occur, which now seems to be well established by cryogenic transmission electron microscopy experiments [10]. Theoretical investigations of the thermodynamics of branched worms have revealed the possibility of coexistence of dilute and dense phases at very low volume fractions. While the earlier theory of Drye and Cates [11] predicts the gas–liquid phase equilibrium only when the strands between branch points consist of very flexible chains, the more recent theory of Kindt [12], substantiated by molecular dynamics simulations, needs rigid chains.

The rheological properties of entangled wormlike micelles may be described by combining reptation theory [13] with a suitable kinetic model describing the scission and recombination of the living polymers. To this end the following processes have been considered [3, 6].

(i) Reversible scission, in which chains break randomly and recombine by end to end fusion.
(ii) End interchange, in which one chain breaks and one of the two products re-combines with a nearby end of a third chain.
(iii) Bond interchange, in which two chains swap a central bond.

The latter two of these lead to a different relaxation of the length distribution after a sudden change in temperature compared to the first one [3, 6], essentially because they preserve the total number of chains. Experiments are weakly in favour of the first mechanism [3]. Assuming this mechanism to be dominant, Cates [14] has investigated its influence on the disentangling of a worm out of its tube, which would have taken a time τ_{rep} had the worm not been capable of reversibly breaking. In cases when the break-up time $\tau_b = 1/(k_1\langle L\rangle)$, with k_1 the scission rate per unit of length, is much smaller than τ_{rep} but large enough to justify the mean field approximation, which assumes that the chain ends have time enough to explore their local environment [15], his theory predicts a mono-exponential decay of the shear relaxation modulus with relaxation time $\tau_R = (\tau_b\tau_{rep})^{1/2}$. An extension of the theory [16] to the case of weakly branched systems retains this mono-exponential decay, but attributes to

it a somewhat smaller decay time τ_R, due to an enhanced curvilinear diffusion of the chains along their tubes. The mono-exponential decay of the shear relaxation modulus has been amply confirmed by experiments [3, 4, 17]. The scaling of rheological properties with volume fraction of surfactant and salt concentration is much more problematic, however [4]. As to salt concentration, there seems to be some consensus that increasing salt concentrations enlarge scission energies, thereby enlarging the viscosity, but finally allowing for branching, thereby lowering the viscosity again.

A few results from nonlinear rheology are relevant for our discussion. With increasing shear rates, dilute aqueous solutions of cetyltrimethyammonium tosylate (CTAT) below φ_{D}^{*} finally approach a critical shear rate above which the viscosity quickly rises to a maximum, which is about ten times as large as the initial viscosity, and then gradually decays again to quite low values [18–20]. Concomitant neutron scattering experiments reveal that above the critical shear rate the micellar rods start to grow with increasing shear rate and finally strongly align with the flow field. Analysis of the position of the first peak of the scattered intensity along the vorticity direction suggests that the shear thickening is due to a shear induced rod–worm transition.

When sheared hard enough, all entangled wormlike micelles finally shear thin by several orders of magnitude. Often the decrease in apparent viscosity occurs over such a small range of stress values that the stress effectively reaches a plateau. Local scattering experiments have revealed [21] the existence of bands of different microstructures in such cases. Recently [22] the velocity profile of a shear banded wormlike micelle in a Couette gap has been measured using heterodyne light scattering. The measurements indicate explicitly the presence of two different bands, a weakly sheared band and one that flows with a high shear rate. On increasing the overall shear rate, the highly sheared band grows progressively at the expense of the low shear band, in agreement with earlier theoretical predictions [23, 24]. The high shear rate band is very fluid and consists of strongly aligned worms.

Only a few particle-based simulations of living polymers have been performed. All of them are based on the so-called FENE-C model [25], which is basically a pearl-necklace chain allowing for the breaking of bonds if their potential energy surpasses a value E_{sc}, and for the recombination of two chains when their ends meet. The solvent consists of single beads of the same size as a monomer. The model is essentially the same as the one used by Cates [14]. It is therefore perfectly suited to investigate the assumptions implicit in Cates's theory, such as the mean field approximation and the assumption that the length distribution is insensitive to the applied shear. In gross terms, the simulations justify these assumptions and confirm the predicted exponential length distribution. It therefore seems appropriate now to set the theory to a more severe test, by simulating a model which allows for as many relaxation mechanisms as are conceivable. In particular, the role of branching in strongly sheared systems should be investigated. In order not to be misled by our limited imagination, we have set ourselves the task of investigating possible 'elementary processes' occurring at points where worms entangle, by performing particle-based simulations appropriate for this particular level of description. In the next section we will describe our model and simulation methods. In section 3 we present our results and discuss their relevance to the rheology of wormlike micelles.

2. Model and simulation methods

Since atomistic simulations of wormlike micelles long enough to sample all modes reasonably well, including the slowest ones, are still out of reach with present day computer power, we have chosen to model the worms at their smallest scale by means of a slightly coarse grained model [26]. The building blocks of this model are still small compared to the typical diameter

of a worm. Each amphiphile consists of one hydrophilic head particle of diameter $(4)^{1/3}\sigma$ and four hydrophobic tail particles of diameter σ [27], bound together by a harmonic potential $\Phi_{\rm bnd}(r_{ij}) = 5000\varepsilon\sigma^{-2}(r_{ij}-\sigma_{ij})^2$, where σ_{ij} is calculated by the usual combination rules. Each tail particle represents about three CH_2 groups. Solvent is simulated by means of spherical particles of diameter σ, each representing about two water molecules. Interactions between like particles, as well as the hydrophilic head–water interactions, are modelled by a Lennard-Jones potential $\Phi_{\rm LJ}(r_{ij}) = 4\varepsilon[(\sigma_{ij}/r_{ij})^{12} - (\sigma_{ij}/r_{ij})^6]$; the hydrophobic tail–water and tail–head interactions are modelled by a purely repulsive potential $\Phi_{\rm rep}(r_{ij}) = \varepsilon(1.05\sigma_{ij}/r_{ij})^9$. These non-bonded forces are implemented in the shifted-force fashion, to smooth the potential near the cut-off radius of $2.5\sigma_{ij}$. All particles have the same mass m. A Nose–Hoover thermostat was used to keep the temperature constant at a value $T = 1.35\varepsilon/k_{\rm B}$ and the density was set to two particles per $3\sigma^3$. The time step was equal to $\tau/500$ with $\tau = (m\sigma^2/\varepsilon)^{1/2}$. A link to experimental values is achieved by $\sigma = 1/3$ nm, $\varepsilon = 2$ kJ mol^{-1} and $m = 36$ g mol^{-1}, in which case $T = 325$ K and $\tau = 1.4$ ps. In a previous simulation [27] we found that the model yields a persistence length of 38σ or 13 nm, which is at the lower side of the experimental range of persistence lengths for wormlike micelles.

The above model is a slight modification of an earlier model [26], in which all particles have the same diameter of 1σ, and which yields stable bi-layers with an area per head group of 23.5 Å^2 and an elasticity coefficient equal to 250 mJ m^{-2} [26, 28, 29]. In a recent study [29] we found that this model gives rise to an edge free energy of 3.9×10^{-11} J m^{-1}, in good agreement with experiments [30]. This model does not produce stable worms, however, because its packing parameter is too high, hence the fourfold increase of the volume of the head group used here [27]. Given the above findings, we are confident that the model faithfully represents a generic amphiphile with enough detail to be used in a 'microscopic' simulation.

To simulate the interactions between two closely entangled worms, the two worms should somehow be forced towards one another. We have chosen here to make a chain of interlocking ring-shaped wormlike micelles, with the chain directed along the z-axis and the rings alternating parallel to the xz and the yz plane. An entanglement arises when the chain is stretched along its axis, i.e. by increasing the length of the periodic simulation box. With regular periodic boundary conditions this requires a box containing one full ring and two half rings. This makes for a rather voluminous simulation box, containing a large number of solvent particles, especially when one realises that the flat shape of the rings cannot be exploited because of the perpendicular orientation of successive rings. Fortunately, a box of half this size suffices when twisted boundary conditions are used, as introduced by Allen and Masters [31] in their simulation of a nematic liquid crystal with a twisting director. The central idea is to connect the face of the simulation box at $-L_z/2$ with the face at $L_z/2$ *after a* 90° *clockwise rotation around the z-axis*, while the two remaining pairs of opposite faces are still coupled by regular periodic boundary conditions. The box now contains only two hemicycles, see figure 1, with the ends pairwise connected by the twisted boundary conditions to form one continuous ring. Although these boundary conditions are fairly simple, their actual implementation in DL_POLY2.0 [32] required numerous changes in various subroutines. One of its consequences is that the x- and y-directions are no longer uniquely defined, hence in the following we will regularly use the terms parallel (to the z-axis) and perpendicular.

For the initial box, the two halves of the worm were created by making two semi-circles, with a radius of 18σ, from 70 slabs of six amphiphiles each. The halves were oriented parallel to the diagonals of the square ground plane of the box, with their centres displaced along the z-axis to form an interlocked configuration. The resulting ring of 840 amphiphiles has an equilibrium length, including thermal undulations, of nearly 130σ [27]. Solvent was added by randomly placing 45 800 particles in the box, rejecting all positions with a large overlap with previously

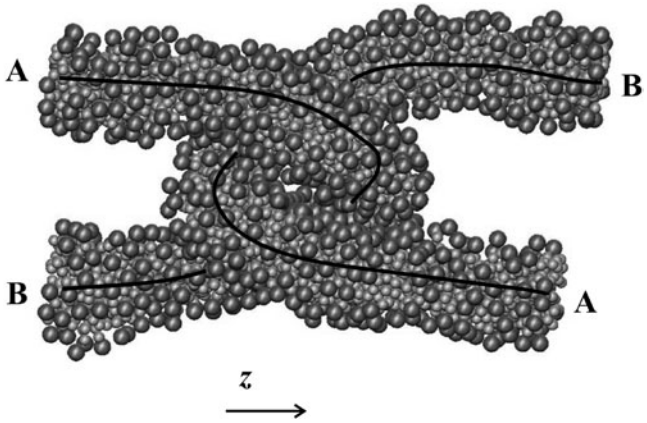

Figure 1. A snapshot of the simulation box containing one self-entangled wormlike micelle. Because of the twisted periodic boundary conditions along the z-axis, the ends marked 'A' are mutually connected, as are the ends marked 'B'. The head and tail particles are two different shades of grey, and are not displayed to size. The solvent has been omitted for clarity. The solid curves serve as a guide to the eye.

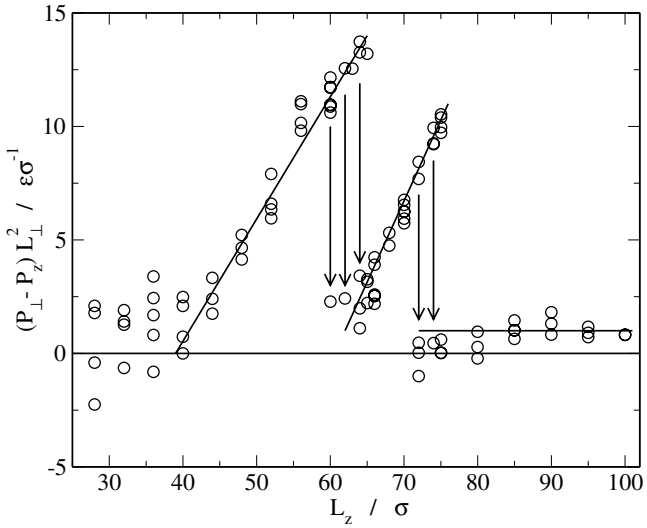

Figure 2. Lateral tension on the box as a function of the length of the simulation box. The lines serve to collect the data points into groups; the arrows indicate some of the observed pressure drops (the average tensions during the transitional runs are not shown). The tension unit $\varepsilon\sigma^{-1}$ along the vertical axis corresponds to 10 pN.

accepted particles. The box was thoroughly equilibrated before the actual production runs started. The simulations showed that this ring, as well as a ring of 450 amphiphiles run with regular boundary conditions, is stable.

3. Results and discussion

Starting with the above described configuration, we stepwise stretched the box along the parallel direction, thereby pulling the worms tightly together, while keeping the total volume of the box constant. In figure 2 we display the lateral tension, i.e. the perpendicular area of the

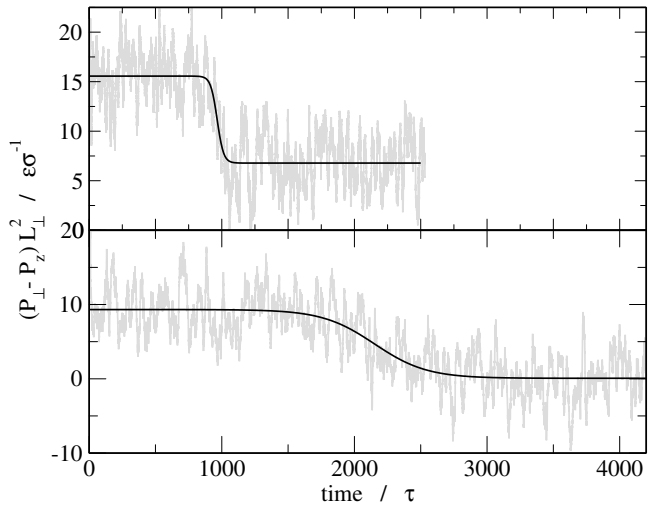

Figure 3. Tension versus time for the transitions at $L_z = 70\sigma$ (top) and 75σ (bottom). The grey line shows a running average over 1000 data points stored at intervals of 0.02τ; the black line is a smooth fit. A period of 1000τ corresponds to 1.4 ns.

box times the difference between the pressures parallel and perpendicular to the z-axis [27], as a function of the strain. The markers represent runs of 1000τ or 1.4 ns (about one week of CPU time) with a fixed box length. After every increment of L_z the box was equilibrated for a similar period, followed by one or more production runs. Several independent boxes with identical L_z were used in the interesting regions of the plot, to verify the reproducibility of the results. After a noisy low tension region, in which the worms occasionally collide because of their Brownian motion, the tension eventually grows linearly with strain as a result of stretching and reduced thermal undulations. Below a box length of 60σ nothing happened to the worms during the sequels of several nanoseconds, and the plot is reversible. But beyond 60σ, for tensions exceeding roughly $11\varepsilon\sigma^{-1}$ or 110 pN, the boxes become unstable and pass through a sharp drop of their tension to a value of about 2 to $3\varepsilon\sigma^{-1}$ or 30 pN. The survival times at these high tension states vary from a fraction of a nanosecond to several nanoseconds, and decrease with increasing tension, indicative of an activated process. On further stretching the relaxed boxes, their tensions again grow linearly up to about $8\varepsilon\sigma^{-1}$ or 80 pN, at which point there is a second drop of the tension, somewhat less abrupt than the first one, to a value of about $1\varepsilon\sigma^{-1}$ or 10 pN. The time evolution of the tension in two typical boxes undergoing these processes is shown in figure 3. Whereas the first process takes place within about 0.2 ns, the second one needs nearly 2 ns to have the tension relaxed to its final value.

In order to better understand what exactly is happening during these two processes, we show in figures 4 and 5 several snapshots of two boxes undergoing these processes. From these figures it is clear that the first tension drop is associated with the merging of the two worms to form an 'H-structure'. It is interesting to note that this step can proceed along two distinct routes. At the highest elongations the worms merge at the back of their respective apices, as one would have expected, but at lower elongations the apex of one worm merges with a point at about the same height on the second worm, as illustrated in figures 4 and 6, presumably after a thermal fluctuation brings the two worms into contact. Although such grazing contacts also happen at lower tensions, we did not observe a single fusion process in the several dozen nanoseconds of simulations run at strains less than $L_z = 60\sigma$, suggesting that the stress on the

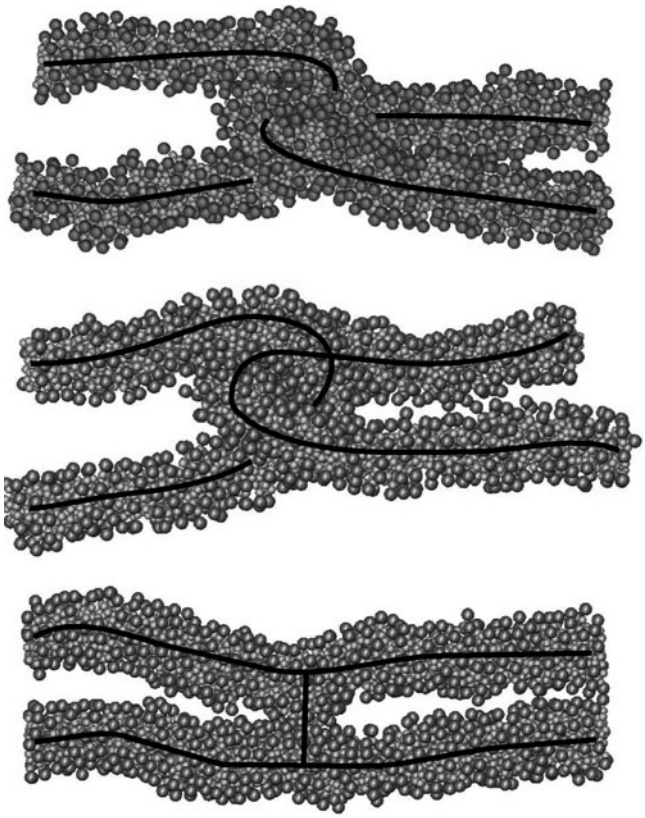

Figure 4. Two 'disconnected' worms merging into an 'H-structure' at $L_z = 66\sigma$, following the second pathway in figure 6.

worm plays an important role in making the worm more receptive to fusion. After merging, stress relaxation and the concomitant splitting of the 'X-junction' into two 'Y-junctions' yields the final stable H-structure. The second tension drop results from the diminishing length of the cross of the H-structure, causing the two Y-junctions to form one X-junction, which then splits under the pressure into the final '2Y-structure'. By gradually shifting the two Y-junctions apart, the system further relaxes its tension, explaining the slow decay in figure 3. This relaxation stops when an equilibrium is reached between the elongational stress on the worm connecting the two Y-junctions and the bending stress on the ring flanked by these two junctions.

Several remarks can be made about these findings. First, we should not give absolute meaning to the size of the first tension drop in figure 3. This merely indicates how much this particular finite system relaxes when it undergoes the corresponding process. Had the box been twice as large as the present one, then the merging would still have occurred at a tension of about 110 pN, but the corresponding tension drop would have been much less than the 80 pN found in the present box. By merging, the worm effectively diminishes its length, thereby relaxing its tension. In a larger box, the loss of length on merging is the same as with the smaller one, but the corresponding tension drop is smaller since it is determined by the relative loss of length. The second process, however, essentially allows the worm to relax its tension to zero. Only when the box is stretched so much that the ring between the two Y-junctions becomes strained will the tension grow again. It is reasonable to expect that finally the ring will disappear and the tension will linearly grow again on stretching the box further. This latter process can hardly be relevant in rheological experiments.

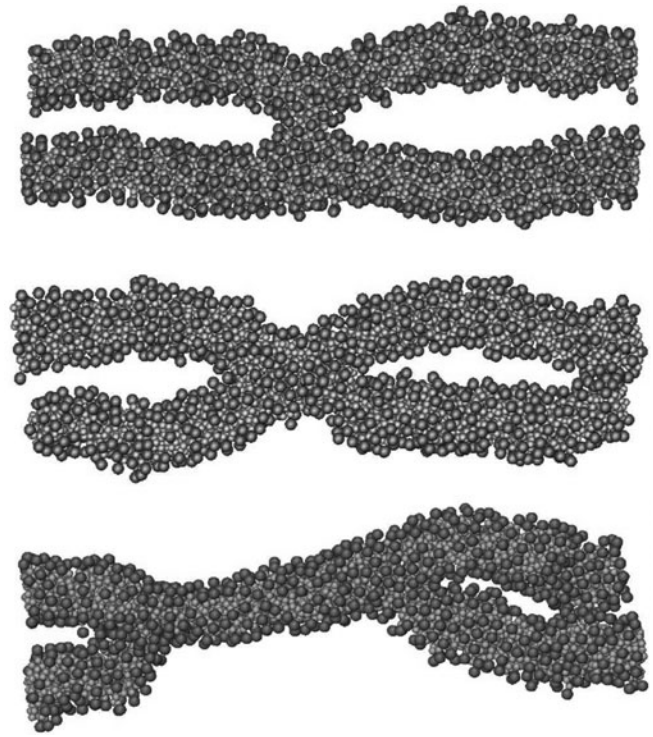

Figure 5. An 'H-structure' breaking up into a '2Y-structure' at $L_z = 75\sigma$. The final state consists of one worm and one ring, with freely moving junctions to minimize the tension.

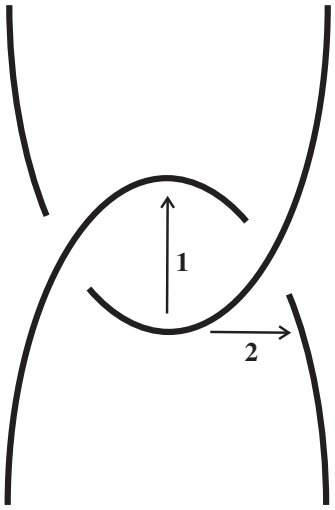

Figure 6. A sketch of two entangled worms (solid curves) and the two routes (arrows) taken during the merging process.

Second, should the worm in our simulations not break instead of merge? Obviously, on using larger and larger boxes, i.e. scaling up the system, eventually the worm will break on stretching. The break-up time for a worm of length L may be written as

$$\tau_{\mathrm{b}}(L) = \alpha_0^{-1} \frac{L_0}{L} \exp\left(\frac{E_0^{\mathrm{a}}}{k_{\mathrm{B}}T}\right),$$

where E_0^{a} is the activation energy for breaking per bond length L_0 in the tensionless state, and α_0^{-1} is a time constant. Since in our simulations the boxes are stretched, the activation energy

must be diminished by W_0, the work done on the box in order to stretch it, divided by the number of bonds. The break-up time $\tau_b(L_{sim})$ of the worm in our simulation then reads

$$\tau_b(L_{sim}) = \frac{\langle L \rangle}{L_{sim}} \tau_b(\langle L \rangle) \exp\left(-\frac{W_0}{k_B T}\right).$$

The work done on the box in order to stretch it up to the point where merging occurs within an accessible simulation time is about 240ε or $180 k_B T$. Now we need a reasonable estimate of the length of an 'elementary' bond. Basically there are three candidates, the diameter of a head group, the diameter of the worm and the persistence length l_p, i.e. 1σ, 7σ and 38σ [27]. Here we choose the diameter of the worm. The total equilibrium length of the material in the box is 130σ, so W_0 is equal to about $10 k_B T$. Reasonable values for the remaining quantities are $\langle L \rangle = 10^{-6}$ m and $\tau_b(\langle L \rangle) = 10^{-1}$ s [3]. Putting everything together we find $\tau_b(L_{sim}) = 1 \times 10^{-4}$ s. We conclude that the break-up time, in the box with the highest tension, is some four orders of magnitude longer than the longest run time, explaining why the worms do not break during our simulations. Notice also that W_0 is still much smaller than the activation energy E_0^a.

Since stresses of 100 pN will not be uncommon in sheared systems, we expect that the simulated process—merging of two entangled worms and subsequent splitting of the fourfold junction into two Y-junctions—will be able to compete with simple breaking of the worms. The mechanism provides a kinetic pathway to the formation of Y-junctions which is much more effective than the attack of a central bond by an end. Moreover, because a relaxation of the tension is easily achieved by adjusting the positions of the two Y-junctions or by the exchange of amphiphiles between the three segments, it is unlikely for the connecting segment to break. This makes the straightforward crossing of worms, process (iii) in the introduction, an improbable event. Note that the observed merging process does not conserve the number of chains, and therefore could agree with the temperature jump experiments.

In sheared systems, one branch of a Y-junction may slide along the other until the Y-junction disappears and a single linear worm results whose length is the sum of the lengths of the two original worms. This may explain the shear-induced growth of worms and corresponding shear thickening found by Berret *et al* [18–20]. It may also explain the extreme lengths and strong alignment of worms at even higher shear rates where shear thinning occurs.

Acknowledgments

This work is part of the research program of the Stichting voor Fundamenteel Onderzoek der Materie (FOM), which is financially supported by the Nederlandse Organisatie voor Wetenschappelijk Onderzoek (NWO). We thank E S Boek and J T Padding for stimulating discussions.

References

[1] Israelachvili J N, Mitchell D J and Ninham B W 1976 Theory of self-assembly of hydrocarbon amphiphiles into micelles and bilayers *J. Chem. Soc. Faraday Trans.* II **72** 1525
[2] Maitland G C 2000 Oil and gas production *Curr. Opin. Colloid Interface Sci.* **5** 301
[3] Cates M E and Candau S J 1990 Statics and dynamics of worm-like surfactant micelles *J. Phys.: Condens. Matter* **2** 6869
[4] Magid L J 1998 The surfactant-polyelectrolyte analogy *J. Phys. Chem.* B **102** 4064
[5] Walker L M 2001 Rheology and structure of worm-like micelles *Curr. Opin. Colloid Interface Sci.* **6** 451
[6] Cates M E 1996 Flow behaviour of entangled surfactant micelles *J. Phys.: Condens. Matter* **8** 9167

[7] Porte G, Gomati R, El Haitamy O, Appell J and Marignan J 1986 Morphological transformations of the primary surfactant structures in brine-rich mixtures of ternary systems (surfactant/alcohol/brine) *J. Phys. Chem.* **90** 5746
[8] Candau S J and Oda R 2001 Linear viscoelasticity of salt-free wormlike micellar solutions *Colloids Surf.* A **183** 5
[9] Khatory A, Lequeux F, Kern F and Candau S J 1993 Linear and nonlinear viscoelasticity of semidilute solutions of wormlike micelles at high salt content *Langmuir* **9** 1456
[10] Croce V, Cosgrove T, Maitland G and Karlsson G 2003 Rheology, cryogenic transmission microscopy, and small-angle neutron scattering of highly viscoelastic wormlike micellar solutions *Langmuir* **19** 8536
[11] Drye T J and Cates M E 1991 Living networks: the role of cross-links in entangled surfactant solutions *J. Chem. Phys.* **96** 1367
[12] Kindt J T 2002 Simulation and theory of self-assembled networks: ends, junctions and loops *J. Phys. Chem.* B **106** 8223
[13] Doi M and Edwards S F 1986 *The Theory of Polymer Dynamics* (Oxford: Oxford University Press)
[14] Cates M E 1986 Reptation of living polymers: dynamics of entangled polymers in the presence of reversible chain-scission reactions *Macromolecules* **20** 2289
[15] O'Shaughnessy B and Yu J 1995 Rheology of wormlike micelles: two universality classes *Phys. Rev. Lett.* **74** 4329
[16] Lequeux F 1992 Reptation of connected wormlike micelles *Europhys. Lett.* **19** 675
[17] Pflaumbaum M and Rehage H 2003 Myristyl dimethylamine oxide surfactant solutions: model systems for rheological research *Chem. Phys. Chem.* **4** 705
[18] Berret J-F, Gamez-Corrales R, Oberdisse J, Walker L M and Lindner P 1998 Flow-structure relationship of shear-thickening surfactant solutions *Europhys. Lett.* **41** 677
[19] Gamez-Corrales R, Berret J-F, Wallker L M and Oberdisse J 1999 Shear-thickening dilute surfactant solutions: equilibrium structures as studied by small-angle neutrons scattering *Langmuir* **15** 6755
[20] Berret J-F, Gamez-Corrales R, Serero Y, Molino F and Lindner P 2001 Shear-induced micellar growth in dilute surfactant solutions *Europhys. Lett.* **54** 605
[21] Schmitt V, Lequeux F, Pousse A and Roux D 1994 Flow behavior and shear induced transition near an isotropic/nematic transition in equilibrium polymers *Langmuir* **10** 955
[22] Salmon J-B, Colin A and Manneville S 2003 Velocity profiles in shear-banding wormlike micelles *Phys. Rev. Lett.* **90** 228303
[23] Spenley N A, Cates M E and McLeish T C B 1993 Nonlinear rheology of wormlike micelles *Phys. Rev. Lett.* **71** 939
[24] Olmsted P D and Lu C-Y D 1997 Coexistence and phase separation in sheared complex fluids *Phys. Rev.* E **56** 55
[25] Kroger M and Makhloufi R 1996 Wormlike micelles under shear flow: a microscopic model studied by nonequilibrium-molecular-dynamics computer simulations *Phys. Rev.* E **53** 2531
[26] Goetz R, Gompper G and Lipwsky R 1999 Mobility and elasticity of self-assembled membranes *Phys. Rev. Lett.* **82** 221
[27] den Otter W K, Shkulipa S A and Briels W J 2003 Buckling and persistence length of an amphiphilic worm from molecular dynamics simulations *J. Chem. Phys.* **119** 2363
[28] den Otter W K and Briels W J 2002 The bending rigidity of an amphiphilic bilayer from equilibrium and nonequilibrium molecular dynamics *J. Chem. Phys.* **118** 4712
[29] Tolpekina T V, den Otter W K and Briels W J 2004 Simulations of stable pores in membranes—system size dependence and line tension *J. Chem. Phys.* submitted
[30] Zhelev D V and Needham D 1993 Tension-stabilized pores in giant vesicles—determination of pore-size and pore line tension *Biochim. Biophys. Acta* **1147** 89
[31] Allen M P and Masters A J 1993 Simulation of a twisted nematic liquid crystal phase *Mol. Phys.* **79** 277
[32] Smith W and Forester T R 1996 A general-purpose parallel molecular dynamics simulation package *J. Mol. Graphics* **14** 136